AIAA JOURNAL
Vol. 44, No. 7, July 2006

Arbitrary Steady-State Solutions with the K–ε Model

C. L. Rumsey*
NASA Langley Research Center, Hampton, Virginia 23681-2199
B. A. Pettersson Reif†
Norwegian Defence Research Establishment, NO-2027 Kjeller, Norway
and
T. B. Gatski‡
NASA Langley Research Center, Hampton, Virginia 23681-2199

Widely used forms of the K–ε turbulence model are shown to yield arbitrary steady-state converged solutions that are highly dependent on numerical considerations such as initial conditions and solution procedure. These solutions contain pseudo-laminar regions of varying size, which can occur even when attempting to use the K–ε model within its intended scope as a fully turbulent computation. By applying a nullcline analysis to the equation set, it is possible to clearly demonstrate the reasons for the anomalous behavior. In summary, use of a low-Reynolds-number damping term in the ε equation causes the degenerate solution to act as a stable fixed point under certain conditions, in turn causing the numerical method to converge there. The analysis also suggests a methodology for preventing the anomalous behavior in steady-state computations.

I. Introduction

THE prediction of turbulent flowfields for engineering purposes continues to be dominated by employing the Reynolds-averaged Navier–Stokes (RANS) approach. Although several classes of closure methodologies are available, the class of two-equation linear eddy viscosity models may be the most popular. Included in this class is the K–ε model, which has many variants. Such models are most effectively utilized when the focus is on mean field dynamics rather than detailed behavior of the statistical moments. The two-equation formulation yields an eddy viscosity that directly influences the mean flow behavior. The K equation can be directly derived from the full Reynolds stress transport equation (by taking the trace). Closure of this K equation then requires a constitutive equation for the Reynolds stress tensor as well as the transport and pressure-diffusion terms. For the Reynolds stress tensor, a linear relation with the mean strain rate tensor is assumed, with the proportionality coefficient being the turbulent eddy viscosity. For the transport and pressure-diffusion terms, gradient transport models are generally assumed. The ε equation is based on transport processes in the dissipative range, but it is often viewed as being an empirical model.[1,2]

Naturally, implicit in the use of all RANS models is the assumption that for a given set of initial and boundary conditions, a unique solution will be obtained. However, it will be shown here that for certain formulations of the K–ε model, portions of the flowfield can converge to a degenerate solution that is pseudo-laminar in nature. The terminology "pseudo-laminar" alludes to the fact that the model does not predict the correct laminar limit in terms of the turbulent to mean flow timescale (SK/ε), but the resulting eddy viscosity is still near zero so the mean flow behaves as a laminar flow. For turbulence model development, the correct limit to consider in the laminar regime is $SK/\varepsilon \gg 1$ [in other words, laminarization occurs as $\varepsilon/(SK) \to 0$; see Durbin and Pettersson-Reif[2]]. In practice, a pseudo-laminar region behaves exactly the same as a laminar region in terms of computational fluid dynamics (CFD) results, but a distinction is made here to draw attention to the fact that the K–ε model is strictly intended only for fully turbulent flows, for which K/ε is well defined and calibrated. When the model predicts near-zero eddy viscosity, this prediction is not based on any real physics. Most significantly, as will be demonstrated, the extent of these pseudo-laminar regions in converged solutions can depend on initial conditions and method of solution! Abid[3] documented a similar sensitivity of the K–ε equations to initial conditions. In Ref. 3, although the equations in some sense responded in a qualitatively correct manner to freestream turbulence level variations (mimicking transition), the method was found to be unreliable due to initial condition sensitivity.

This paper both demonstrates the problem and performs an analysis that explains why the system of equations behaves in this manner. It should be noted that this anomalous behavior occurs only in developing flows, i.e., boundary layers. Flow configurations that utilize streamwise periodic boundary conditions (such as fully developed channel flow) do not in general encounter this problem. It should also be noted that although the anomalous behavior may be influenced to some degree by such factors as the rate of freestream turbulence decay (inherent in the K–ε equations) or by the "stagnation point anomaly" (see Durbin[4]), the problem persists regardless, due to the nature of the equations themselves.

The purpose of this analysis is to critically examine the characteristics of the K–ε model from a dynamical systems standpoint. Mohammadi and Pironneau[5] reported extensive mathematical analysis on the K–ε model but did not consider the anomalies described here. Dynamical system analyses have previously been utilized[6–8] to identify the fixed points of two-equation and second-moment closures in homogeneous shear flow and to calibrate closure models for equilibrium flows. The issues addressed in the present study, however, require that the evolution toward the equilibrium state is understood, particularly the solution trajectories from a given initial condition, and not the fixed points per se. Although the theoretical approach is inherently based on the simplifying assumption of homogeneous turbulence, an attempt is also made to account for

Received 3 June 2005; revision received 6 September 2005; accepted for publication 9 September 2005.

*Senior Research Scientist, Computational Aerosciences Branch; c.l.rumsey@nasa.gov. Associate Fellow AIAA.

†Senior Scientist, P.O. Box 25; also Adjunct Professor, Department of Applied Mechanics, Chalmers University of Technology, SE-41296 Gothenburg, Sweden; bjorn.reif@ffi.no. Member AIAA.

‡Senior Research Scientist, Computational Aerosciences Branch; currently Research Director, B.P. 30179, Laboratoire d'Études Aérodynamiques, UMR CNRS 6609, Université de Poitiers, SP2MI, Téléport 2, Bd. Marie et Pierre Curie, 86962 Futuroscope, Chasseneuil Cedex, France; also Research Professor, Department of Ocean, Earth and Atmospheric Sciences, Old Dominion University, Norfolk, VA 23529; t.b.gatski@widomaker.com. Associate Fellow AIAA.

inhomogeneous effects so that the theoretical results can be more easily related to the full numerical solution of the model in realistic wall-bounded flows.

As already alluded to, the dynamical systems analysis undertaken here is concerned not only with fixed-point identification but also with dependent variable phase-plane trajectories and dependence on initial conditions. The analysis isolates the characteristics in some formulations of the K–ε model that lead to initial condition and solution-method–dependent converged solutions.

II. Illustration of the Problem

To illustrate the anomalies arising in numerical solutions of the K–ε model, two cases are considered: 1) a flat plate boundary-layer flow and 2) flow over an airfoil. The computer code CFL3D[9] was employed. (Another code, ISAAC,[10] has been used and yields anomalous results.) As will be shown, the capacity to reach arbitrary steady-state solutions is a property of certain forms of the K–ε equations themselves, and so any numerical method using these forms will encounter the problem.

A basic form of the K–ε model can be written as

$$\frac{\mathrm{D}K}{\mathrm{D}t} = \mathcal{P} - \varepsilon + \frac{\partial}{\partial x_j}\left[\left(\nu + \frac{\nu_t}{\sigma_K}\right)\frac{\partial K}{\partial x_j}\right] \tag{1a}$$

$$\frac{\mathrm{D}\varepsilon}{\mathrm{D}t} = \frac{\varepsilon}{K}(C_{\varepsilon 1}\mathcal{P} - f_2 C_{\varepsilon 2}\varepsilon) + \frac{\partial}{\partial x_j}\left[\left(\nu + \frac{\nu_t}{\sigma_\varepsilon}\right)\frac{\partial \varepsilon}{\partial x_j}\right] \tag{1b}$$

where $\mathrm{D}/\mathrm{D}t = \partial/\partial t + U_j \partial/\partial x_j$, $C_{\varepsilon 1} = 1.44$, $C_{\varepsilon 2} = 1.83$, $\sigma_K = 1.0$, $\sigma_\varepsilon = \kappa^2/[\sqrt{C_\mu}(C_{\varepsilon 2} - C_{\varepsilon 1})]$, $\kappa = 0.41$, and $C_\mu = 0.09$. The set of values used here for the closure constants are representative of values typically chosen. However, as will be seen, the anomalous behavior exists regardless of their exact numerical values. The rate of turbulent energy production $\mathcal{P}$ is defined as $-\overline{u_i u_j}\,\partial U_i/\partial x_j$, and the components of the Reynolds stress tensor are modeled using the Boussinesq assumption:

$$\overline{u_i u_j} = \frac{2}{3}K\delta_{ij} - \nu_t\left(\frac{\partial u_i}{\partial x_j} + \frac{\partial u_j}{\partial x_i}\right) \tag{2}$$

with the eddy viscosity given by

$$\nu_t = f_\mu C_\mu (K^2/\varepsilon) \tag{3}$$

In this type of formulation, the damping function f_2 is introduced into Eq. (1b) so that as a solid boundary is approached the destruction-of-dissipation term does not become ill-behaved.[11] It is also used to calibrate the model in the log-layer region. For example, two widely used forms for f_2 are

$$f_2 = 1 - c_1 \exp\left(-c_2 Re_T^2\right) \tag{4}$$

where $Re_T = K^2/(\nu\varepsilon)$, and

$$f_2 = 1 - c_3 \exp(-c_4 Re_K) \tag{5}$$

where $Re_K = \sqrt{K}d/\nu$ and d is the distance from the wall. The constants c_1 and c_3 are always positive and less than or equal to 1.0, and c_2 and c_4 are positive constants. Note that $1 - c_1 \le f_2 \le 1$ for Eq. (4) and $1 - c_3 \le f_2 \le 1$ for Eq. (5). For the present demonstrations, only Eq. (5) was used, with the values $c_3 = 1$, $c_4 = 2/25$, but Eq. (4) exhibits similar behavior. Also, to simplify the subsequent analysis, the second damping function f_μ is taken here to be 1. With the other constants used, the resulting solution in the turbulent region still yields excellent agreement with the law-of-the-wall log layer (Fig. 1), as well as with wall skin friction. Using more standard forms for f_μ has some effects, including improved asymptotic behavior very near the wall, but the overall anomalous behavior of the equations still exists. In fact, as will be shown in Sec. III.E, the f_μ term has no influence on whether the anomalous behavior occurs.

To rule out the possibility that the observed arbitrary behavior occurred only for a particular set of boundary conditions, various freestream boundary conditions for K and ε were employed. The anomalies occurred regardless of these variations, as will be exemplified. Because the solutions were highly dependent on numerical parameters, the grid size itself could also have an influence on the final solution. Reasonably fine grids were used for both cases, but a formal grid independence study was not conducted because it has no meaning when the equations themselves (and not the numerics) can yield arbitrary results.

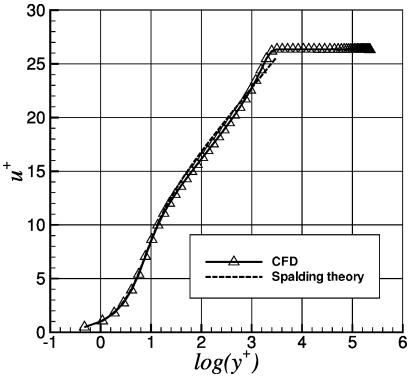

Fig. 1 Example flat plate log-layer solution in the turbulent regime.

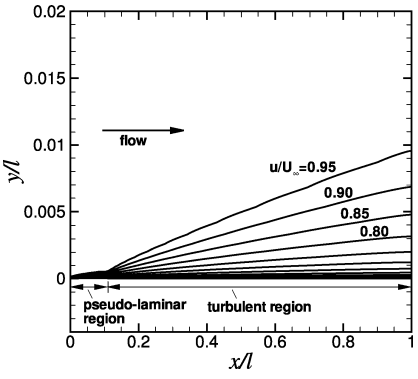

Fig. 2 Example flat plate solution showing u/U_∞ contours for initial condition $\varepsilon_0' = 8.1\,K_0'$; $M_\infty = 0.2$, $Re = 6.0 \times 10^6$ (l = length of plate).

A. Flat Plate Boundary Layer

In the flat plate boundary-layer flow considered first, a freestream turbulent intensity of 0.2% [$= \sqrt{(2K_\infty/3u_\infty^2)}$] was imposed everywhere in the computational domain using a grid of 193×65 at a Reynolds number (based on plate length) of $Re = 6 \times 10^6$. Thus, the initial condition K_0 on K was everywhere the same as the boundary condition ($K_0' = K_\infty' = K_\infty/u_\infty^2 = 6.0 \times 10^{-6}$). The dissipation rate boundary condition at inflow, which determines the freestream eddy viscosity and turbulence freestream decay rate, was set at $\varepsilon_\infty l/u_\infty^3 = 8.1 K_\infty/u_\infty^2$, or $\varepsilon_\infty' = 8.1 K_\infty'$. This yielded a freestream eddy viscosity for this case of $\mu_t/\mu_\infty = 0.40$ at the boundaries. A sample solution showing the final u/U_∞-velocity contours is plotted in Fig. 2, for the case with initial condition $\varepsilon_0' = 8.1 K_0'$. The solution exhibited a pseudo-laminar solution upstream of $x/l \approx 0.1$ and then a turbulent solution downstream. Next, different cases were run with four different initial conditions ε_0' in the field varying from 0.0081 to $81 K_0'$.

As Fig. 3 shows, each converged solution yielded a different apparent "transition" location that was located farther downstream with increasing initial dissipation rate values. At sufficiently high levels ($\varepsilon_0' = 81 K_0'$), the flow remained laminar throughout. Initially, this might seem like consistent behavior: an increased dissipation should reduce the level of turbulent kinetic energy K and therefore should shift the position of transition farther downstream. However, this rationale is flawed for two reasons, one more serious than the other from a CFD practitioner's point of view.

First, in the presence of mean shear (e.g., $S = \partial U/\partial y$), a laminar solution is characterized by very large values of the time-scale ratio, i.e., $SK/\varepsilon \gg 1$. Physically this implies that the turbulent timescale

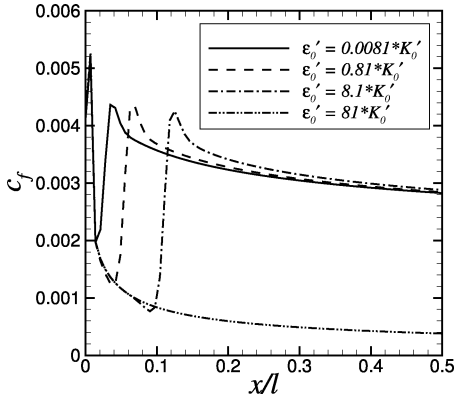

Fig. 3 Streamwise variation of skin-friction coefficient on front half of flat plate as a function of initial conditions ($K_0' = 6.0 \times 10^{-6}$).

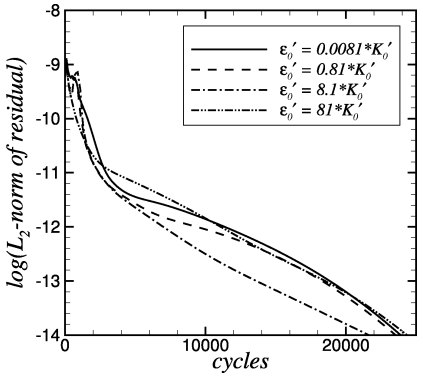

Fig. 4 Convergence history for flat plate computations.

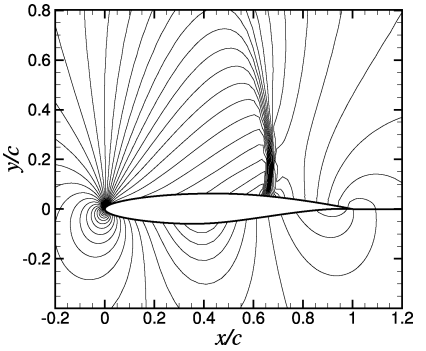

Fig. 5 Example RAE 2822 airfoil solution showing static pressure contours; $M_\infty = 0.75$, $\alpha = 2.72$, $Re = 6.2 \times 10^6$ (c = chord length).

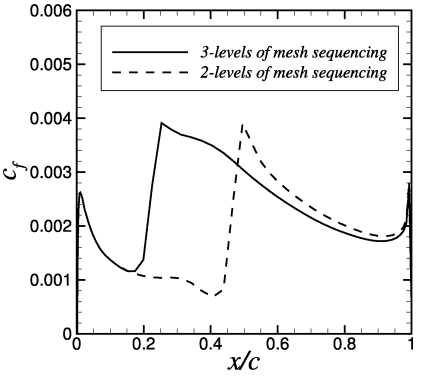

Fig. 6 Streamwise variation of skin-friction coefficient on RAE 2822 airfoil lower surface for two different solution procedures. (The procedures converged.)

is much greater than the mean flow timescale and as such turbulence does not persist. But inspection of the "laminar" regions in the current solution shows that SK/ε is in fact $\ll 1$. In other words, the K–ε model is not really predicting laminar flow at all, but rather a pseudo-laminar behavior that will be shown in Sec. III to be a stable fixed point of the equations.

Second, and even more serious, is that the final converged solution should not depend on the initial condition in a steady-state computation at all! The converged solution should depend on the boundary conditions only, and in this case the boundary conditions were the same in all computations. It should be stressed that the solutions presented in Fig. 3 were very well converged solutions. The L_2 norm of the density residual dropped by more than six orders of magnitude, to approximately 1×10^{-14}, as shown in Fig. 4. The solutions after 25,000 multigrid cycles showed no perceptible differences from those solutions obtained after 2500 cycles.

B. RAE 2822 Airfoil

As a second example of anomalous behavior, the flow over an RAE 2822 airfoil at freestream Mach number $M_\infty = 0.75$, angle of attack $\alpha = 2.72$, and $Re = 6.2 \times 10^6$ was computed. A plot showing the airfoil shape and resulting pressure contours for these conditions is given in Fig. 5. There is a strong shock wave present on the airfoil upper surface near 65% chord, whereas the flow on the lower surface remains subsonic. In this example, the initial and boundary conditions were kept fixed but the numerical solution method was changed. The initial conditions and far-field boundary conditions in this case were set to $K'_\infty = 2.5 \times 10^{-8}$ and $\varepsilon'_\infty = 3.75 \times 10^{-8}$. This corresponded to a very low freestream turbulent intensity of 0.013% and a freestream eddy viscosity of $\mu_t/\mu_\infty = 0.009$. These are typical values used in CFL3D.[9]

Figure 6 shows the skin-friction distribution on the lower surface of the airfoil obtained using two different numerical solution strategies for obtaining converged solutions. The converged results were completely different, with each suggesting a transition location in a different place. The first case was run using multigrid and three levels of mesh sequencing, with 2500 iterations on the coarse grid, followed by 2500 iterations on the medium grid, and finally 3000 iterations on the finest grid (257×97). The second case was run with multigrid and two levels of mesh sequencing, with 5000 iterations on the medium grid followed by 3000 iterations on the finest grid. Although not shown, both cases converged very well, with the L_2 norm of density residual reduced more than three orders of magnitude.

Both these examples show that caution needs to be exercised when using the K–ε model. A numerically converged solution does not necessarily constitute the intended solution to the set of governing equations; it may depend on numerical parameters such as initial conditions and solution procedure. It is also important to mention here that many CFD practitioners have noticed that the K–ε equations often fail to go fully turbulent, although the cause has never been identified before. In fact, it is customary to build in ad hoc fixes to attempt to ensure that turbulence always develops. Some of these fixes include 1) restarting K–ε solutions from another turbulent solution, 2) setting initial conditions to have turbulent-like levels rather than freestream levels, and 3) imposing a temporary source term in the boundary layer to trip turbulence. All of these fixes, in general, are workable ways to avoid the problem, but they do not shed any light on the reasons behind the problem and were not developed based on any firm rational foundation. As a consequence, their generality cannot be assured. In the following section an analysis is conducted that makes the reasons clear.

III. Dynamical Systems Analysis

A dynamical systems analysis can be used to determine the temporal dynamics associated with the numerical solution of systems of equations.[12] A so-called nullcline analysis will also be used to identify some parametric restrictions on the K–ε equations (1) to avoid arbitrary pseudo-laminar converged solutions.

A. Analysis of Homogeneous Form

It is possible to gain critical insight into the solution behavior for inhomogeneous turbulent flows through an analysis of the

homogeneous form of Eq. (1). The assumption of homogeneous flows in turbulence model development is very useful because the log layer or equilibrium layer of a turbulent boundary layer has the same dynamical characteristics as a homogeneous flow. We exploit this dynamic similarity here by treating the flow as "locally homogeneous" in the boundary layer. In other words, although the mean shear varies throughout a boundary layer, we make the assumption of a locally fixed mean shear value at a given location. Although this assumption is crude, CFD computations given later in Sec. III.C confirm its approximate validity and usefulness in the analysis of the problem. In its homogeneous limit, Eq. (1) can be written as a nonlinear, autonomous equation system in the form

$$\frac{\mathrm{d}K^*}{\mathrm{d}t^*} = C_\mu \frac{K^{*2}}{\varepsilon} - \varepsilon \tag{6a}$$

$$\frac{\mathrm{d}\varepsilon}{\mathrm{d}t^*} = C_{\varepsilon 1} C_\mu K^* - f_2 C_{\varepsilon 2} \frac{\varepsilon^2}{K^*} \tag{6b}$$

where, for convenience, we define $K^* \equiv SK$ ($S \equiv \partial u/\partial y$ to be fixed and assumed to be finite in the analysis) and $t^* \equiv St$. There can be either one or two critical points in this system: 1) the null vector with elements $K^* = \varepsilon = 0$, and 2), if it exists, the intersection of the set of points with $\mathrm{d}K^*/\mathrm{d}t^* = 0$ that lie on the K^* nullcline described by

$$\varepsilon = \pm\sqrt{C_\mu} K^* \tag{7a}$$

and the set of points with $\mathrm{d}\varepsilon/\mathrm{d}t^* = 0$ that lie on the ε nullcline described by

$$\varepsilon = \pm\sqrt{\frac{C_\mu C_{\varepsilon 1}}{f_2 C_{\varepsilon 2}}} K^* \tag{7b}$$

Realizability considerations dictate that only the positive roots need to be considered. At the intersection point of Eqs. (7a) and (7b), $f_2 = C_{\varepsilon 1}/C_{\varepsilon 2}$. Thus, this second critical point exists only if f_2 can achieve a value $C_{\varepsilon 1}/C_{\varepsilon 2}$ (which for the current set of closure coefficients is 0.7869). From Eq. (4) or (5), this means that critical point 2 can exist only if $c_1 \geq 1 - C_{\varepsilon 1}/C_{\varepsilon 2}$ or $c_3 \geq 1 - C_{\varepsilon 1}/C_{\varepsilon 2}$ for these particular choices of f_2.

If stable, the critical points represent the possible steady-state solutions to the system, Eq. (6). Note that neither of these critical points (1 or 2) is the so-called "turbulent" solution. In the analysis of homogeneous turbulent flow, the turbulent solution grows without bound ($K^* \to \infty$). The reason the analysis yields an unbounded growth in this case is that the mean flowfield is fixed and unaffected by the turbulence, and this provides an infinite source of energy for the turbulence. In practical computations, this behavior is not seen because there is a two-way coupling between the turbulent and mean flowfields. The coupling allows for a turbulent steady state to be reached. Diffusion, to be introduced later in the analysis, also plays an important role in practical computations.

The stability properties of the two critical points can be examined by linearizing about each critical point. The coefficient matrix of this linear system is the Jacobian matrix

$$J = \begin{bmatrix} 2C_\mu\left(\dfrac{K^*}{\varepsilon}\right) & -C_\mu\left(\dfrac{K^*}{\varepsilon}\right)^2 - 1 \\ C_\mu C_{\varepsilon 1} + f_2 C_{\varepsilon 2}\left(\dfrac{\varepsilon}{K^*}\right)^2 - C_{\varepsilon 2}\left(\dfrac{\varepsilon^2}{K^*}\right)\dfrac{\partial f_2}{\partial K^*} & -2f_2 C_{\varepsilon 2}\left(\dfrac{\varepsilon}{K^*}\right) - C_{\varepsilon 2}\left(\dfrac{\varepsilon^2}{K^*}\right)\dfrac{\partial f_2}{\partial \varepsilon} \end{bmatrix} \tag{8}$$

To determine the nature of the critical points (e.g., whether they are stable or unstable), the eigenvalues of this matrix are found at the critical points. Table 1 lists the possible types. A center indicates that trajectories orbit around the critical point. A stable critical point means that, when solving the equations, the particular point can be reached; an unstable critical point or a saddle point means that a numerical scheme will not converge to it. (A saddle point is not stable in practice because orbits approach the critical point along one eigenvector, but then recede along the eigenvector associated with the unstable solution.)

Table 1 Type of critical point as determined by eigenvalues of *J*

Type of eigenvalue	Critical point type
Complex with zero real part	Center
Complex with negative real part	Stable focus
Complex with positive real part	Unstable focus
Real and both negative	Stable node
Real and both positive	Unstable node
Real with one positive, one negative	Saddle point

It can be shown that, when it exists, critical point 2 of the system equation (6) is always a saddle point. When Eq. (4) is used for f_2, the eigenvectors at the saddle point are

$$\begin{bmatrix} \boldsymbol{X}_1 \\ \boldsymbol{X}_2 \end{bmatrix} = \begin{bmatrix} 2 \\ \sqrt{C_\mu}(1 + C_{\varepsilon 1}) + C_{\varepsilon 2}\sqrt{C_\mu} D\,\ell_n(B) \pm \sqrt{A} \end{bmatrix} \tag{9}$$

where $A = C_\mu(1 - C_{\varepsilon 1})^2 + C_\mu C_{\varepsilon 2} D^2\,\ell_n^2(B) + 8C_\mu C_{\varepsilon 2} D(C_{\varepsilon 1} - 3)\,\ell_n(B)$, $B = (C_{\varepsilon 2} - C_{\varepsilon 1})/(c_1 C_{\varepsilon 2})$, and $D = 1 - C_{\varepsilon 1}/C_{\varepsilon 2}$. When Eq. (5) is used for f_2, the eigenvectors at the saddle point are

$$\begin{bmatrix} \boldsymbol{X}_1 \\ \boldsymbol{X}_2 \end{bmatrix} = \begin{bmatrix} 2 \\ \sqrt{C_\mu}(1 + C_{\varepsilon 1}) \pm \sqrt{C_\mu(1 - C_{\varepsilon 1})^2 - C_\mu C_{\varepsilon 2} D\,\ell_n(E)} \end{bmatrix} \tag{10}$$

where $E = (C_{\varepsilon 2} - C_{\varepsilon 1})/(c_3 C_{\varepsilon 2})$. The effect of the saddle point on the solution trajectories will be shown later when phase plots are drawn. But the more interesting critical point in this analysis is the first degenerate one ($K^* = \varepsilon = 0$), which corresponds to a pseudo-laminar solution. When Eq. (4) or (5) is used for f_2, and if the condition

$$K^*/\varepsilon \ll 1 \tag{11}$$

as $K^* = \varepsilon = 0$ is approached, is true, then this degenerate point can be a stable point. This stability of the degenerate critical point turns out to be the cause of the apparently arbitrary solution behavior demonstrated in Sec. II.

In Sec. III.D, the conditions for which Eq. (11) occur will be explored in greater detail. It will also be shown that stability of the degenerate point requires the second critical (saddle) point to exist. For now, however, the assertion is made that in practice Eq. (11) is quite often true for the system of equations given by Eq. (1) or (6). As a result, $Re_T \ll 1$ and $Re_K \ll 1$ near the critical point as well. Therefore, for $1 - c_1$ not small, Eq. (4) is approximately $f_2 = 1 - c_1$, and for $c_1 = 1$ it is approximately $f_2 = c_2 K^{*4}/(S^4 \nu^2 \varepsilon^2)$. Similarly, for $1 - c_3$ not small, Eq. (5) is approximately $f_2 = 1 - c_3$, and for $c_3 = 1$ it is approximately $f_2 = c_4 K^{*1/2} d/(\nu S^{1/2})$. Using these expressions, along with expressions for the derivatives of Eqs. (4) and (5) with respect to K^* and ε, the eigenvalues of the matrix in Eq. (8) near the degenerate critical point can be determined. These are given in Table 2 for the two f_2 expressions and various combinations of their coefficients. In most cases, the degenerate critical point is stable. [The "center" type of critical point is also not desirable in this context, because solutions can become locked in an orbit and fail to converge. However, no known models actually use

Table 2 Eigenvalues near the $K^* = \varepsilon = 0$ critical point, with $K^*/\varepsilon \ll 1$[a]

f_2 Function ($c_2, c_4 > 0$)	Type of eigenvalue	Critical point type
$1 - c_1 \exp(-c_2 Re_T^2)$, $c_1 = 1$	Complex, near-zero real part	Center
$1 - c_1 \exp(-c_2 Re_T^2)$, $0 < c_1 < 1$	Real, both negative for $c_1 < (C_{\varepsilon 2} - 1)/C_{\varepsilon 2}$	Stable node
	Complex, negative real part for $c_1 > (C_{\varepsilon 2} - 1)/C_{\varepsilon 2}$	Stable focus
$1 - c_3 \exp(-c_4 Re_K)$, $c_3 = 1$	Complex, negative real part for $\mathcal{P}/\varepsilon < C_{\varepsilon 2} c_4 Re_K$,	Stable focus
	Complex, near-zero real part for $\mathcal{P}/\varepsilon > C_{\varepsilon 2} c_4 Re_K$	Center
$1 - c_3 \exp(-c_4 Re_K)$, $0 < c_3 < 1$	Real, both negative for $c_3 < (C_{\varepsilon 2} - 1)/C_{\varepsilon 2}$	Stable node
	Complex, negative real part for $c_3 > (C_{\varepsilon 2} - 1)/C_{\varepsilon 2}$	Stable focus

[a]The computations in Sec. II employed a model that corresponds to the third alternative.

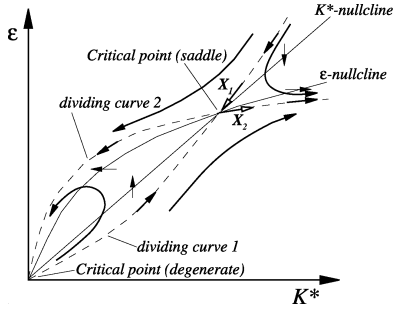

Fig. 7 Sketch of nullclines and critical points from Eqs. (7a) and (7b) and resulting K^*–ε phase diagram ($K^* = SK$); dividing curves (dashed lines) divide trajectories near critical points.

$c_1 = 1$ in Eq. (4), and so from now on the analysis focuses only on the more common cases in which the critical point is stable.] A second center type in Table 2 occurs using Eq. (5) with $c_3 = 1$, when $\mathcal{P}/\varepsilon = C_\mu K^{*2}/\varepsilon^2 > C_{\varepsilon 2} c_4 Re_K$. But with sufficiently small K^* relative to $\varepsilon^{4/3}$, this inequality is not satisfied and the critical point remains stable.

Equations (7a) and (7b) can be sketched for a case in which the two nullclines intersect. Inspection of Eqs. (6a) and (6b) then shows the following to apply:

$$\frac{dK^*}{dt^*} = 0, \text{ on Eq. (7a)}, \qquad \frac{dK^*}{dt^*} < 0, \text{ left of Eq. (7a)}$$

$$\frac{dK^*}{dt^*} > 0, \text{ right of Eq. (7a)} \tag{12a}$$

$$\frac{d\varepsilon}{dt^*} = 0, \text{ on Eq. (7b)}, \qquad \frac{d\varepsilon}{dt^*} < 0, \text{ above Eq. (7b)}$$

$$\frac{d\varepsilon}{dt^*} > 0, \text{ below Eq. (7b)} \tag{12b}$$

Combining this information with the knowledge of the behavior at the critical points, a clear mapping of the phase-plane trajectories can be drawn, as shown in Fig. 7. The eigenvectors ($\boldsymbol{X}_1, \boldsymbol{X}_2$) at the saddle point are shown along with dividing curves (dashed lines) that separate regions of different trajectory behavior. Clearly, any initial condition above dividing curve 1 converges toward the degenerate critical point.

An actual phase-plane portrait can be constructed by computing the right-hand sides of Eqs. (6) for a large number of K^* and ε values. These computed values then correspond to $\partial K^*/\partial t^*$ and $\partial \varepsilon/\partial t^*$ at each particular point in nondimensional K^*–ε phase space, and the trajectory (how K^* and ε change with time or with iteration) can be computed as well.

An example is shown in Fig. 8, using Eq. (5) for f_2 with $c_3 = 1$, $c_4 = 2/25$, $S' = 1569$, $d' = 2.945 \times 10^{-4}$. [Typical results with Eq. (4) yield a similar behavior.] The nullclines are shown along with the phase space trajectories. It is clear that this figure matches the sketch in Fig. 7 in character: $K^* = \varepsilon = 0$ is a stable attractor, and the other critical point (near $K^* = 0.19$, $\varepsilon = 0.057$ in this particular case) is a saddle point. The true turbulent solution is obtained when K^* grows (exponentially); in other words, the expected turbulent solution occurs only when the K^* and ε values follow the trajectories in

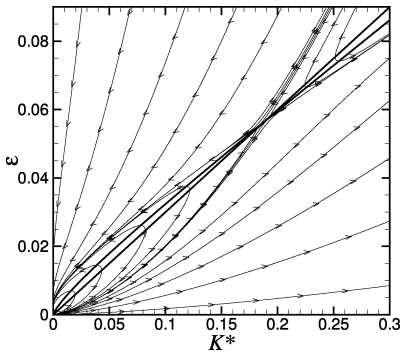

Fig. 8 Example phase-plane portrait of Eq. (6) showing nullclines (two oblique lines going from lower left to upper right) and trajectories (lines with arrows) with f_2 given by Eq. (5).

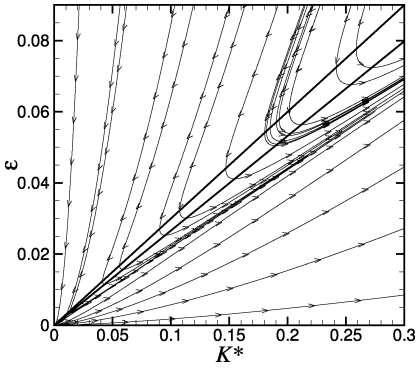

Fig. 9 Example phase-plane portrait of Eq. (6) showing nullclines (two oblique lines going from lower left to upper right) and trajectories (lines with arrows) with $f_2 = 1$.

the lower-right or far-upper-right-hand parts of the plot. This figure demonstrates that there are many regions in the map for which the solution converges toward the degenerate critical point $K^* = \varepsilon = 0$.

It is also interesting to look at the phase space trajectories of the case with $f_2 = 1$, shown in Fig. 9. Here, the two nullclines do not cross, and so there is no saddle point (i.e., no second critical point). The trajectories now behave like the ones to the right of the saddle point in Fig. 8; regardless of the initial condition, the solution always goes to the turbulent solution and never to the degenerate one. This figure suggests that the f_2 damping function is responsible for the anomalous pseudo-laminar behavior.

B. Accounting for Diffusion

Inhomogeneous effects that necessarily occur in any practical calculation can be represented by the viscous diffusion term and the gradient diffusion models for the turbulent transport, represented by ν_t/σ_K and ν_t/σ_ε. Because the consideration here is for high-Reynolds-number flows, viscous diffusion effects can be neglected in the turbulent region, and it is necessary only to adequately represent the effects of the turbulent transport in both the kinetic energy and energy dissipation rate equations. It suffices for the purposes here to simply assume that the transport effects act over a distance l given by $K^{3/2}/\varepsilon$. Thus, qualitative estimates for the transport terms

can be written as

$$\frac{\partial}{\partial x_j}\left(\frac{\nu_t}{\sigma_K}\frac{\partial K}{\partial x_j}\right) \sim \mathcal{O}\left(\frac{K^3}{\varepsilon l^2}\right) \sim \mathcal{O}(\varepsilon) = C^*_{\mu K}\varepsilon \qquad (13a)$$

$$\frac{\partial}{\partial x_j}\left(\frac{\nu_t}{\sigma_\varepsilon}\frac{\partial \varepsilon}{\partial x_j}\right) \sim \mathcal{O}\left(\frac{K^2}{l^2}\right) \sim \mathcal{O}\left(\frac{\varepsilon^2}{K}\right) = C^*_{\mu\varepsilon}\frac{\varepsilon^2}{K} \qquad (13b)$$

with $C^*_{\mu K}$ and $C^*_{\mu\varepsilon}$ as unknown coefficients. Using these estimates for the transport terms allows them to be grouped with the destruction terms. Thus, an equation set that accounts for inhomogeneity can be written as

$$\frac{\mathrm{d}K^*}{\mathrm{d}t^*} = C_\mu\frac{K^{*2}}{\varepsilon} - \left(1 - C^*_{\mu K}\right)\varepsilon \qquad (14a)$$

$$\frac{\mathrm{d}\varepsilon}{\mathrm{d}t^*} = C_{\varepsilon 1}C_\mu K^* - \left(f_2 C_{\varepsilon 2} - C^*_{\mu\varepsilon}\right)\frac{\varepsilon^2}{K^*} \qquad (14b)$$

It is clear to see that the effect of the additional diffusion-type terms is merely to tilt the nullclines up, making them steeper. As will be shown in Sec. III.C, this effect is needed to achieve agreement between theory and computation. The relative shapes and positions of the phase space trajectories are a function of the relative magnitudes of the a priori unknown) $C^*_{\mu K}$ and $C^*_{\mu\varepsilon}$. In this case, the nullclines intersect to form a saddle point when $f_2 = [C_{\varepsilon 1}(1 - C^*_{\mu K}) + C^*_{\mu\varepsilon}]/C_{\varepsilon 2}$.

C. Comparison of Computations with Analysis

Through the foregoing analysis, it is clear that the equations themselves (when they contain an f_2 function in the ε-equation destruction term) can cause degenerate solutions to occur. But how well does the theory compare with actual RANS computations? Although the actual RANS computations are much more complicated than the analytical model because the mean flow S and the actual diffusion terms vary in time and space, we can look at these varying values at specific points from the earlier flat plate computation, for example, and choose representative levels over the latter part of the temporal development. These representative levels can then be inserted into Eq. (14) when computing the theoretical phase-space trajectories for comparison.

Figures 10 and 11 show the results using this procedure at two different points in the flowfield. Figure 10 shows computed results at a point in the boundary layer that eventually converged to a pseudo-laminar degenerate result, along with the theoretical trajectories. Here, diffusion effects were negligible, and there is excellent agreement between theory and computation. Figure 11 is for a point farther downstream that became fully turbulent. Here, the effect of diffusion was important and needed to be taken into account in the theory; values used for $C^*_{\mu K}$ and $C^*_{\mu\varepsilon}$ were 0.28 and 0.59, respectively, based on representative levels seen in the flat plate computation. There is again excellent agreement between theory and computation.

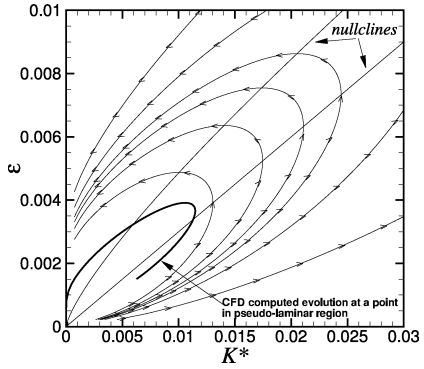

Fig. 10 Comparison of theory with computed result at a point in pseudo-laminar region of the flat plate computation.

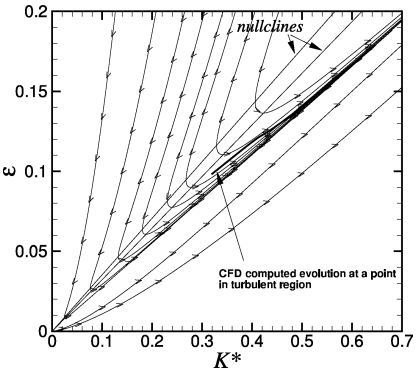

Fig. 11 Comparison of theory with computed result at a point in turbulent region of the flat plate computation.

D. Avoiding Arbitrary Steady-State Solutions

Earlier, Eq. 11 was given as a condition for which the degenerate critical point was either a center or a stable point. The interrelationship between this condition and the value of f_2 is now explored. Consider the equation for K^*/ε:

$$\frac{\mathrm{d}(K^*/\varepsilon)}{\mathrm{d}t^*} = -\frac{\mathcal{P}}{\varepsilon}(C_{\varepsilon 1} - 1) - (1 - C_{\varepsilon 2}f_2) \qquad (15)$$

where $\mathcal{P}/\varepsilon = C_\mu K^{*2}/\varepsilon^2$. From this equation it is immediately apparent that for $\mathrm{d}(K^*/\varepsilon)/\mathrm{d}t^* < 0$ (which must be true for K^*/ε to be driven toward zero), the following must hold:

$$f_2 < \frac{\mathcal{P}}{\varepsilon}\frac{C_{\varepsilon 1} - 1}{C_{\varepsilon 2}} + \frac{1}{C_{\varepsilon 2}} \qquad (16)$$

If this inequality is not satisfied, then K^*/ε remains nonzero, and the eigenvalue analysis of the Jacobian matrix equation (8) shows that the $K^* = \varepsilon = 0$ critical point is always unstable and no longer an attractor for the degenerate solution. This suggests a method to avoid the problem of arbitrary solutions for steady-state computations: compute f_2 as usual with Eq. (4) or (5), but then limit it via

$$f_2' = \min\left[1, \max\left(f_2, \frac{\mathcal{P}}{\varepsilon}\frac{C_{\varepsilon 1} - 1}{C_{\varepsilon 2}} + \frac{1}{C_{\varepsilon 2}}\right)\right] \qquad (17)$$

during the early transient stages of a steady-state computation. This limiter does not allow the value of f_2 to go below the critical level defined by Eq. (16). Once turbulence has been established, the limiter can be removed. This analysis does not lead to a method for avoiding arbitrary solutions in time-dependent computations. Such computations are prone to anomalous behavior as well.

Another important observation is that the right-hand side in Eq. (16) is less than $C_{\varepsilon 1}/C_{\varepsilon 2}$ for $\mathcal{P}/\varepsilon < 1$. Because the second critical (saddle) point exists only if f_2 can achieve a value $C_{\varepsilon 1}/C_{\varepsilon 2}$, this implies that a second critical point is necessary for the degenerate point ($K^* = \varepsilon = 0$) to be stable, when using the current equation set.

E. Extension to More General Form

To summarize, the analysis suggests that the presence of two critical points for a commonly used form of the K–ε equations has the potential to produce anomalous pseudo-laminar behavior. The degenerate point associated with the pseudo-laminar solution ($K^*/\varepsilon \ll 1$; $K^* = \varepsilon = 0$) is stable only if there exists a second critical point given by $f_2 = C_{\varepsilon 1}/C_{\varepsilon 2}$.

One can write the homogeneous limit of the K–ε equations in more general form:

$$\frac{\mathrm{d}K^*}{\mathrm{d}t^*} = C^*_\mu\frac{K^{*2}}{\varepsilon} - \varepsilon \qquad (18a)$$

$$\frac{\mathrm{d}\varepsilon}{\mathrm{d}t^*} = \frac{\varepsilon}{K^*}\left(C^*_{\varepsilon 1}C^*_\mu\frac{K^{*2}}{\varepsilon} - C^*_{\varepsilon 2}\varepsilon\right) \qquad (18b)$$

where the new variables C_μ^*, $C_{\varepsilon 1}^*$, and $C_{\varepsilon 2}^*$ can now each include functions of the solution. (For example, low-Reynolds-number models[11] often use a function f_μ that is included here in the term C_μ^*.) In the more general form of Eq. (18), the second critical point is now defined by

$$C_{\varepsilon 2}^* = C_{\varepsilon 1}^* \tag{19}$$

which is independent of C_μ^*. The analysis strongly suggests that any K–ε model for which $C_{\varepsilon 2}^* \leq C_{\varepsilon 1}^*$ somewhere in the flow has the potential to yield an arbitrary pseudo-laminar solution.

IV. Conclusions

A peculiar problem inherent in a widely used form of the K–ε turbulence model has been demonstrated and analyzed. This problem has a potentially large impact on practical CFD computations. Use of an f_2 function multiplying the destruction term of the dissipation rate equation was shown to cause portions of the flowfield to converge to a degenerate pseudo-laminar condition. Most disturbingly, this condition is highly dependent on numerical parameters such as initial conditions and solution procedure. In other words, RANS solutions using this particular form of the K–ε model can easily yield arbitrary fully converged solutions with pseudo-laminar regions of varying size. These arbitrary solutions can occur even when attempting to use the K–ε model within its intended scope as a fully turbulent computation. Time-dependent computations are also susceptible to the anomalous behavior.

A nullcline analysis was used to analyze the homogeneous form of the equations, followed by a form that approximately accounts for the effect of diffusion. The analysis clearly demonstrated the reasons for the anomalous behavior of this turbulence model: the degenerate solution was a stable fixed point under certain conditions, causing the numerical method to converge there. The analysis also led to a methodology for preventing the anomalous behavior in steady-state solutions by using the current equation set.

The results presented here also suggested that any K–ε model for which the coefficient multiplying the destruction term in the ε equation can be less than or equal to the coefficient multiplying the production term has the potential to produce arbitrary pseudo-laminar solutions.

References

[1]Pope, S. B., *Turbulent Flows*, Cambridge Univ. Press, Cambridge, England, U.K., 2000, p. 375.

[2]Durbin, P., and Pettersson-Reif, B. A., *Statistical Theory and Modeling of Turbulent Flows*, Wiley, New York, 2001, Chaps. 6 and 8.

[3]Abid, R., "Evaluation of Two-Equation Turbulence Models for Predicting Transitional Flows," *International Journal of Engineering Science*, Vol. 31, No. 6, 1993, pp. 831–840.

[4]Durbin, P. A., "On the K–ε Stagnation Point Anomaly," *International Journal of Heat and Fluid Flow*, Vol. 17, No. 1, 1996, pp. 89, 90.

[5]Mohammadi, B., and Pironneau, O., *Analysis of the K–Epsilon Turbulence Model*, Wiley, Chichester, England, U.K., 1994.

[6]Speziale, C. G., and Mhuiris, N. M. G., "On the Prediction of Equilibrium States in Homogeneous Turbulence," *Journal of Fluid Mechanics*, Vol. 209, 1989, pp. 591–615.

[7]Speziale, C. G., Gatski, T. B., and Mhuiris, N. M. G., "A Critical Comparison of Turbulence Models for Homogeneous Shear Flows in a Rotating Frame," *Physics of Fluids A*, Vol. 2, No. 9, 1990, pp. 1678–1684.

[8]Speziale, C. G., Sarkar, S., and Gatski, T. B., "Modelling the Pressure-Strain Correlation of Turbulence: An Invariant dynamical Systems Approach," *Journal of Fluid Mechanics*, Vol. 227, 1991, pp. 245–272.

[9]Krist, S. L., Biedron, R. T., and Rumsey, C. L., "CFL3D User's Manual (Version 5.0)," NASA TM-1998-208444, June 1998.

[10]Morrison, J. H., "Flux Difference Split Scheme for Turbulent Transport Equations," AIAA Paper 90-5251, 1990.

[11]Patel, V. C., Rodi, W., and Scheuerer, G., "Turbulence Models for Near-Wall and Low Reynolds Number Flows: A Review," *AIAA Journal*, Vol. 23, No. 9, 1985, pp. 1308–1319.

[12]Gerstner, W., and Kistler, W. M., *Spiking Neuron Models, Single Neurons, Populations, Plasticity*, Cambridge Univ. Press, Cambridge, England, U.K., 2002.

C. Kaplan
Associate Editor